INTERNATIONAL JOURNAL FOR NUMERICAL METHODS IN FLUIDS, VOL. 6, 65–82 (1986)

IMPROVED AVERAGING METHOD FOR TURBULENT FLOW SIMULATION. PART II: CALCULATIONS AND VERIFICATION

YOUSSEF M. DAKHOUL

Continuum, Inc., Huntsville, Alabama, U.S.A.

AND

KEITH W. BEDFORD

Civil Engineering Department, The Ohio State University, Columbus, Ohio, U.S.A.

SUMMARY

This is the second of two articles intended to develop, apply and verify a new method for averaging the momentum and mass transport equations for turbulence. Part I presented the theoretical development of a new space-time filter (STF) averaging procedure. The new method, as well as all existing averaging procedures, are applied to the one-dimensional transient equations of momentum and scalar transport in a Burgers' flow field. Dense-grid 'exact' results from the unaveraged equations are presented to depict the dynamic behaviour of the flow field and serve as a basis for verifying the coarse-grid STF predictions. In this paper, a finite difference procedure is used to numerically solve the new STF averaged equations, as well as the other forms of the averaged equations derived in Part I. All averaged equations are solved on the same coarse grid. The velocity and scalar fields, predicted from each equation form, are intercompared according to a verification procedure based on the statistical and spectral properties of the results. It is found that the new STF procedure improves coarse-grid dynamic predictions over the existing methods of averaging.

KEY WORDS Turbulence Modelling Large Eddy Simulation Filtering One-Dimensional Scalar Transport Burgers' Flow

INTRODUCTION

In the first paper of this series a new space-time filter (STF) was derived and used to average the one-dimensional Burgers-type equations for momentum and scalar transport. As part of this development, other existing methods of spatial or temporal averaging were reviewed and also used to average one-dimensional Burgers forms of the momentum and scalar transport equations. Since dynamically varying Burgers solutions are to be used to test the STF filter, an 'exact' solution for such a case was identified and calculated by a dense grid finite difference procedure. The grid used in the 'exact' solution fully resolved all the time and space fluctuations in the flow field.

The purpose of this paper is to solve the new STF averaged equations on a coarse grid, and evaluate the performance of the method by comparison to data from the dense grid solution. Prior to the comparison, the dense grid solution is averaged commensurate with the scale sizes inherent in the STF filter. The performance of the other averaging procedures is similarly evaluated, and all results are intercompared by means of checks on the ability of the models to reproduce the

0271–2091/86/020065–18$09.00

Received 14 January 1985
Revised 6 September 1985

Table I. The average Burgers' equation

Unaveraged (A1)	$\frac{\partial u}{\partial t}+\frac{1}{2}\frac{\partial}{\partial x}[uu]$	$=\nu\frac{\partial^2 u}{\partial x^2}$
Reynolds averaging (A2)	$\frac{\partial \bar{u}}{\partial t}+\frac{1}{2}\frac{\partial}{\partial x}[\bar{u}\bar{u}]$	$=\nu\frac{\partial^2 \bar{u}}{\partial x^2}-\frac{1}{2}\frac{\partial}{\partial x}\left\{\overline{u'u'}\right\}$
Uniform spatial averaging	$\frac{\partial \bar{u}}{\partial t}+\frac{1}{2}\frac{\partial}{\partial x}[\bar{u}\bar{u}]$	$=\nu\frac{\partial^2 \bar{u}}{\partial x^2}-\frac{1}{2}\frac{\partial}{\partial x}\left\{(\overline{\bar{u}\bar{u}}-\bar{u}\bar{u})+\overline{2\bar{u}u'}+\overline{u'u'}\right\}$
Leonard's averaging	$\frac{\partial \bar{u}}{\partial t}+\frac{1}{2}\frac{\partial}{\partial x}\left[\bar{u}\bar{u}+\frac{\Delta_x^2}{4\gamma}\frac{\partial^2\bar{u}\bar{u}}{\partial x^2}\right]$	$=\nu\frac{\partial^2 \bar{u}}{\partial x^2}-\frac{1}{2}\frac{\partial}{\partial x}\left\{\overline{2\bar{u}u'}+\overline{u'u'}\right\}$
Leonard's averaging and Clark's reduction (A3)	$\frac{\partial \bar{u}}{\partial t}+\frac{1}{2}\frac{\partial}{\partial x}\left[\bar{u}\bar{u}+\frac{\Delta_x^2}{2\gamma}\frac{\partial \bar{u}^2}{\partial x}\right]$	$=\nu\frac{\partial^2 \bar{u}}{\partial x^2}-\frac{1}{2}\frac{\partial}{\partial x}\left\{\overline{u'u'}\right\}$
STF	$\frac{\partial \bar{u}}{\partial t}+\frac{1}{2}\frac{\partial}{\partial x}\left[\bar{u}\bar{u}+\frac{\Delta_t^2}{4\gamma}\frac{\partial^2\bar{u}\bar{u}}{\partial t^2}+\frac{\Delta_x^2}{4\gamma}\frac{\partial^2\bar{u}\bar{u}}{\partial x^2}\right]$	$=\nu\frac{\partial^2 \bar{u}}{\partial x^2}-\frac{1}{2}\frac{\partial}{\partial x}\left\{\overline{2\bar{u}u'}+\overline{u'u'}\right\}$
STF with Clark's reduction (A4-A6)	$\frac{\partial \bar{u}}{\partial t}+\frac{1}{2}\frac{\partial}{\partial x}\left[\bar{u}\bar{u}+\frac{\Delta_t^2}{2\gamma}\frac{\partial \bar{u}^2}{\partial t}+\frac{\Delta_x^2}{2\gamma}\frac{\partial \bar{u}^2}{\partial x}\right]$	$=\frac{\partial^2 \bar{u}}{\partial x^2}-\frac{1}{2}\frac{\partial}{\partial x}\left\{\overline{u'u'}\right\}$

Table II. Averaged one-dimensional scalar transport equation

Unaveraged (A1)	$\frac{\partial c}{\partial c}+\frac{\partial}{\partial x}[uc]$	$=\alpha\frac{\partial^2 c}{\partial x^2}$
Reynolds averaging (A2)	$\frac{\partial \bar{c}}{\partial t}+\frac{\partial}{\partial x}[\bar{u}\bar{c}]$	$=\alpha\frac{\partial^2 \bar{c}}{\partial x^2}-\frac{\partial}{\partial x}\left\{\overline{u'c'}\right\}$
Uniform spatial Averaging	$\frac{\partial \bar{c}}{\partial t}+\frac{\partial}{\partial x}[\bar{u}\bar{c}]$	$=\alpha\frac{\partial^2 \bar{c}}{\partial x^2}-\frac{\partial}{\partial x}\left\{(\overline{\bar{u}\bar{c}}-\bar{u}\bar{c})+\overline{\bar{u}c'}+\overline{u'\bar{c}}+\overline{u'c'}\right\}$
Leonard's averaging	$\frac{\partial \bar{c}}{\partial t}+\frac{\partial}{\partial x}\left[\bar{u}\bar{c}+\frac{\Delta_x^2}{4\gamma}\frac{\partial^2\bar{u}\bar{c}}{\partial x^2}\right]$	$=\alpha\frac{\partial^2 \bar{c}}{\partial x^2}-\frac{\partial}{\partial x}\left\{\overline{\bar{u}c'}+\overline{u'\bar{c}}+\overline{u'c'}\right\}$
Leonard's averaging with Clark's Averaging (A3)	$\frac{\partial \bar{c}}{\partial t}+\frac{\partial}{\partial x}\left[\bar{u}\bar{c}+\frac{\Delta_x^2}{2\gamma}\frac{\partial \bar{u}}{\partial x}\frac{\partial \bar{c}}{\partial x}\right]$	$=\alpha\frac{\partial^2 \bar{c}}{\partial x^2}-\frac{\partial}{\partial x}\left\{\overline{u'c'}\right\}$
STF	$\frac{\partial \bar{c}}{\partial t}+\frac{\partial}{\partial x}\left[\bar{u}\bar{c}+\frac{\Delta_t^2}{4\gamma}\frac{\partial^2\bar{u}\bar{c}}{\partial t^2}+\frac{\Delta_x^2}{4\gamma}\frac{\partial^2\bar{u}\bar{c}}{\partial x^2}\right]$	$=\alpha\frac{\partial^2 \bar{c}}{\partial x^2}-\frac{\partial}{\partial x}\left\{\overline{\bar{u}c'}+\overline{u'\bar{c}}+\overline{u'u'}\right\}$
STF with Clark's reduction (A4–A6)	$\frac{\partial \bar{c}}{\partial t}+\frac{\partial}{\partial x}\left[\bar{u}\bar{c}+\frac{\Delta_t^2}{2\gamma}\frac{\partial \bar{u}}{\partial t}\frac{\partial \bar{c}}{\partial t}+\frac{\Delta_x^2}{2\gamma}\frac{\partial \bar{u}}{\partial x}\frac{\partial \bar{c}}{\partial x}\right]$	$=\alpha\frac{\partial^2 \bar{c}}{\partial x^2}-\frac{\partial}{\partial x}\left\{\overline{u'c'}\right\}$

Table III. The energy equation

Averaging Procedure	Term no.					
	LHS	1	2	3	4	5
Unaveraged	$\frac{\partial}{\partial t}\left\langle \frac{v^2}{2} \right\rangle$	$= -\frac{1}{2}\left\langle v\frac{\partial v^2}{\partial x}\right\rangle$			$+\nu\left\langle v\frac{\partial^2 v}{\partial x^2}\right\rangle$	
Reynolds averaging	$\frac{\partial}{\partial t}\left\langle \frac{v^2}{2} \right\rangle$	$= -\frac{1}{2}\left\langle v\frac{\partial v^2}{\partial x}\right\rangle$			$+\nu\left\langle v\frac{\partial^2 v}{\partial x^2}\right\rangle$	$+\frac{1}{2}\left\langle v\frac{\partial}{\partial x}\left(k\frac{\partial v}{\partial x}\right)\right\rangle$
Leonard's averaging with Clark's reduction	$\frac{\partial}{\partial t}\left\langle \frac{v^2}{2} \right\rangle$	$= -\frac{1}{2}\left\langle v\frac{\partial v^2}{\partial x}\right\rangle$		$-\frac{\Delta x^2}{4\gamma}\left\langle v\frac{\partial}{\partial x}\left(\frac{\partial v}{\partial x}\right)^2\right\rangle$	$+\nu\left\langle v\frac{\partial^2 v}{\partial x^2}\right\rangle$	$+\frac{1}{2}\left\langle v\frac{\partial}{\partial x}\left(k\frac{\partial v}{\partial x}\right)\right\rangle$
STF with Clark's reduction	$\frac{\partial}{\partial t}\left\langle \frac{v^2}{2} \right\rangle$	$= -\frac{1}{2}\left\langle v\frac{\partial v^2}{\partial x}\right\rangle$ $-\frac{\Delta_t^2}{4\gamma}\left\langle v\frac{\partial}{\partial x}\left(\frac{\partial v}{\partial t}\right)^2\right\rangle$		$-\frac{\Delta_x^2}{4\gamma}\left\langle v\frac{\partial}{\partial x}\left(\frac{\partial v}{\partial x}\right)^2\right\rangle$	$+\nu\left\langle v\frac{\partial^2 v}{\partial x^2}\right\rangle$	$+\frac{1}{2}\left\langle v\frac{\partial}{\partial x}\left(k\frac{\partial v}{\partial x}\right)\right\rangle$

v is the velocity u minus its spatial average.
For complete derivation see Reference 6.

statistical and spectral details of the exact solution. A comparison of energy distribution and transfer is also performed.

MODEL EQUATIONS

Governing transport equations

The one-dimensional Burgers' flow and passive scalar transport equations are derived in the first paper using seven different forms of space or time averaging. Tables I and II contain the equations. The new STF filtered equations are the sixth and seventh forms. Here the overbars denote averaging according to whatever averaging definition was used. The Δs are filter coefficients to be specified later. In Tables I and II, the residuals resulting from averaging have not been closed.

Residual closure

To close the residual terms $\overline{u'u'}$ and $\overline{u'c'}$, the Boussinesq concept is used, i.e.

$$\overline{u'u'} = -K(\partial\bar{u}/\partial x), \tag{1}$$

$$\overline{u'c'} = -D(\partial\bar{c}/\partial x). \tag{2}$$

K is an eddy viscosity and D is an eddy diffusivity related to K by a turbulent Schmidt number $S_t = K/D$. For K, the following model is used to calculate the local instantaneous values:

$$K = C_r\delta_x^2|\overline{\partial\bar{u}/\partial x}|^{\frac{p}{w}}, \tag{3}$$

where C_r is a non-dimensional residual field coefficient, δ_x is the spatial grid spacing and the overbars denote averaging over a length w and a time period p. When $w = 0$ and $p = 0$, equation (3) is a one-dimensional analog of the Smagorinsky model.[1-3] In the limit $w = L$ (the total length of the solution domain) equation (3) is analogous to the direct interaction closure used by Leslie and Quarini[4] and Love and Leslie.[5] The values for w, p and C_r are selected in subsequent sections.

Energy equation

As part of the verification procedure, the energy equations derived from each of the momentum equations in Table I are depicted in Table III. The energy equation is derived by multiplying each term in the respective momentum equation by the velocity, and taking an ensemble average, which is denoted by $\langle\,\rangle$. The equations are derived using the residual closure forms as in the previous section. After solution for the velocity field, the size of each numbered term in the energy equation is estimated by numerical discretization and used to create time histories which are then compared to the time histories from the exact solution.

NUMERICAL PROCEDURE

In analogy to References 4 and 5, an explicit finite difference scheme is used to solve the equations in Tables I and II, and estimate the size of the individual terms in Table III. Complete details are found in Reference 6. The scheme ensures overall fourth order accuracy for the non-linear terms, which is required because of their importance in transferring turbulent energy and propagating the steep gradients in the turbulent variables. The viscosity and diffusivity terms are discretized by usual second-order accurate central schemes.

The Adams–Bashforth method was selected to calculate the advance in time. The method is explicit, second order accurate in time and weakly unstable.[7] Because it uses information at three time levels, it may develop computational modes the severity of which depends on the grid spacings. This problem is controlled by the size of the grid spacings.

MODEL IMPLEMENTATION

Selection of fixed input parameters

The total length of the one-dimensional simulation domain is chosen to be 12 L where L is an arbitrary unit of length. The total time of simulation is one arbitrary unit of time, T. For the 'exact' or dense-grid calculation the length 12 L is divided into 4026 equal intervals, and the time T into 2013 equal time steps. These grid spacings are small enough to resolve all the spatial and temporal scales in the unaveraged quantities typically calculated in this research.

The Schmidt numbers are unity, so that the molecular diffusivity, α, is equal to the molecular viscosity, ν. Also, the eddy diffusivity, D, is set equal to the eddy viscosity, K, though it may in fact be different. For all coarse-grid calculations, the spatial filter width, Δ_x, is equal to $2\delta_x$ where δ_x is the spatial grid spacing. The residual field coefficient, C_r, is set equal to 4·0. These values have been optimized by Love[8] who used the Leonard's averaging scheme.

The values of w and p, in equation (3), are initially set equal to 14 δ_t and 14δ_x, respectively. Here δ_t is the time step size. The length w is bisected by the node under consideration and the period p includes the uncentred previous 14 time steps so that the solution procedure remains explicit. The tests used to optimize the values of w and p are presented in a later section.

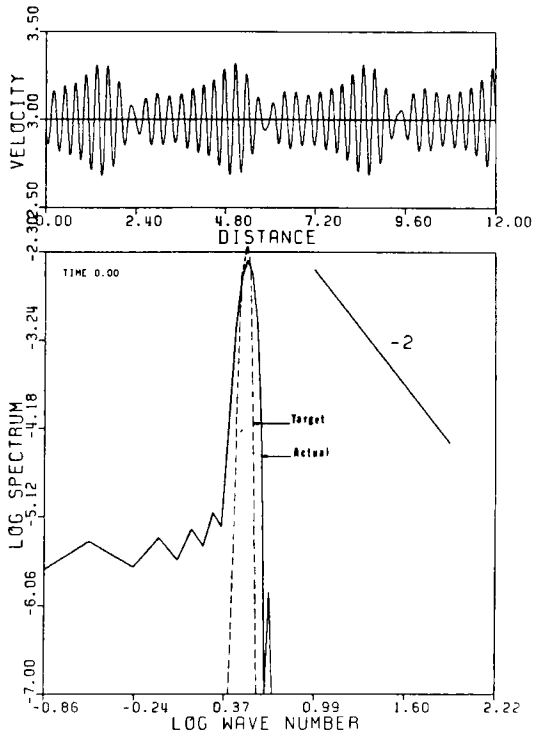

Figure 1. Momentum field initial condition

Initial and boundary conditions

The initial velocity distribution is a discrete random signal in x. The signal is generated as described by Shinozuka and Jan[9] with target and actual wave number (ω) spectra as shown in Figure 1. Note that the inertial subrange is devoid of any significant spectrum values. This makes it possible to observe the gradual development, at later time steps, of a spectral distribution with the expected ω^{-2} dependency in the inertial subrange. The spectrum in Figure 1 has a maximum at $\log \omega = 0{\cdot}5235$; thus the most significant length scale, L_0, is $(1/\log^{-1} 0{\cdot}5235)$ or $0{\cdot}299\, L$, and the most significant velocity scale, V_0, is the mean of $u(x, 0)$, which is equal to $3{\cdot}0\, L/T$. The molecular viscosity, ν, is then determined by

$$\nu = L_0 V_0 / R_n = 0{\cdot}908/R_n(L^2/T), \tag{4}$$

where R_n is the variable Reynolds number.

The initial concentration field is uniform over the spatial flow field and equal to one arbitrary unit of concentration. This makes it possible to observe how the scalar 'pollutant' is convected by the velocity field. For solving both the momentum and concentration equations, the periodic boundary conditions are used:

$$u(x, t) = u(x + 12L, t), \tag{5}$$

$$c(x, t) = c(x + 12L, t). \tag{6}$$

Experiments performed

An extensive series of numerical experiments was performed to test the new filter against existing filters, and the results presented in this paper will concentrate on comparing the various filters in calculating a known flow with a Burgers' Reynolds number of 500. Since the time filter width is a new and unknown variable, additional test results are presented to demonstrate the sensitivity of the results to its size. Table IV lists the coarse grid numerical experiments and its first column contains the run numbers which will appear next to all the curves depicting the results. In Table IV, Δ_t is the temporal filter width, R_n is the Reynolds number and N and M are the numbers of nodes and time steps, respectively.

Output presentation procedure

The unaveraged equations are first solved on a fine grid using the data given earlier in this section and a Reynolds number of 500. The resulting 'exact' u and c fields are averaged to extract the $\bar{u}$ and $\bar{c}$

Table IV. Coarse grid simulations for evaluating the averaging method

Run number	Averaging method	Δ_t	R_n	N	M
A1	——	0			
A2	Reynolds	0			
A3	Leonard's	0	500	806	470
A4	STF	$4\delta_t$			
A5	STF	$8\delta_t$			
A6	STF	$10\delta_t$			

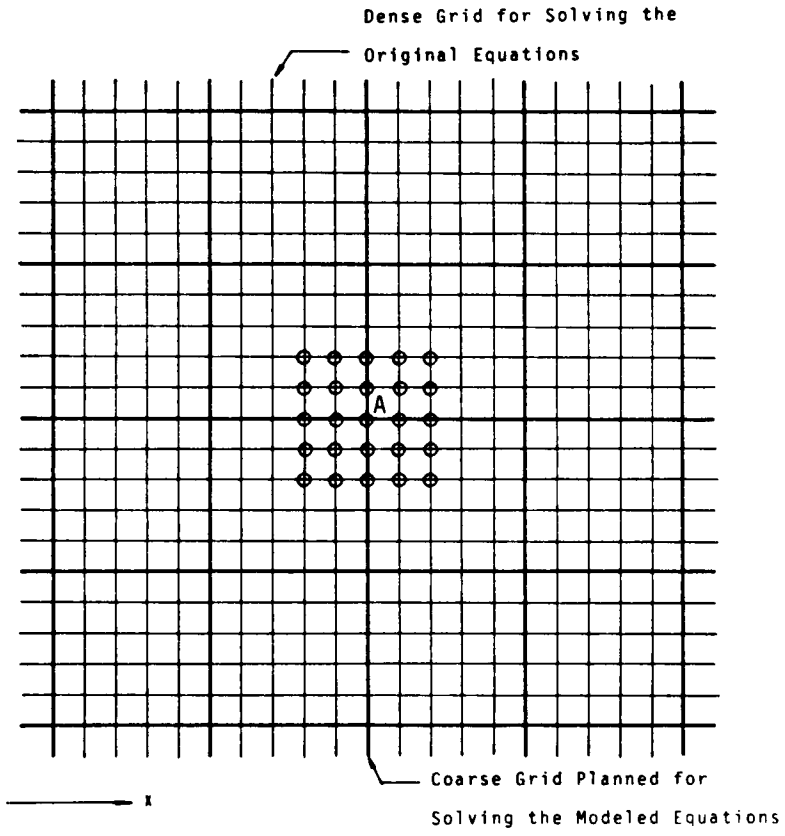

Figure 2. Grid definitions for large scale averaging

fields commensurate with the grid spacings of Table IV. Ideally, this extraction should be done via the same averaging operations used to derive the averaged equations. The averaged equations, however, are solved repeatedly using three different averaging methods and a wide range of filter widths. As an approximation, the extraction will be done following the procedure of Clark *et al.*[10] In this procedure, the large-scale component of a certain variable at point A (Figure 2) is simply the arithmetic average of the exact values at the circled nodes on the dense grid. The $\bar{u}$ and $\bar{c}$ fields thus obtained are called the 'exact-averaged' fields and are used to verify the $\bar{u}$ and $\bar{c}$ fields obtained from the runs listed in Table IV.

The verification involves comparing time histories of $\bar{u}$ and $\bar{c}$ at fixed locations and spatial distributions at certain time steps, as well as the following statistics: (1) wave number spectra of the spatial distributions at certain time instants, (2) frequency spectra of the time signals at specified spatial locations and (3) time histories of the spatial variance, skewness and kurtosis. Also, as a part of the verification procedure for Table IV runs, the time histories of the energy terms (Table III) are plotted. The purpose of these plots is to observe the relative size of each of the terms and their role in the energy field balance.

For a general (space or time) signal, α_i, consisting of N points ($i = 1, 2, \ldots, N$) with a spacing δ between the points, the statistics mentioned above are calculated as follows:

$$\text{Mean} = (1/N) \sum_{i=1}^{N} \alpha_i, \tag{7}$$

$$\text{Variance} = (1/N)\sum_{i=1}^{N}(\alpha_i - \text{Mean})^2, \tag{8}$$

$$\text{Skewness} = \left[\sum_{i=1}^{N}(\alpha_i - \text{Mean})^3\right] \Big/ [N(\text{Variance})^{3/2}], \tag{9}$$

$$\text{Kurtosis} = \left[\sum_{i=1}^{N}(\alpha_i - \text{Mean})^4\right] \Big/ [N(\text{Variance})^2], \tag{10}$$

$$\text{Spectrum}_j = (2\delta/\pi)\sum_{k=1}^{\text{NS}} \varepsilon_k R_k \cos[(j-1)(k-1)\pi/(\text{NS}-1)], \tag{11}$$

$$\text{Wave number}_j \text{ or frequency}_j = (j-1)/[2\delta(\text{NS}-1)], \tag{12}$$

where

$$\begin{aligned} \varepsilon_k &= 1/2 \quad (\text{for } k = 1, \text{NS}) \\ &= 1 \quad (\text{for } k = 2, 3, \ldots, \text{NS}-1). \end{aligned} \tag{13}$$

R_k stands for the autocorrelations:

$$R_k = [1/(N-K+1)]\sum_{l=1}^{N-k+1}(\alpha_l - \text{Mean})(\alpha_{l+k-1} - \text{Mean}). \tag{14}$$

The index j takes the values $1, 2, \ldots,$ NS where NS is the required number of points in the computed spectrum. NS is usually chosen within the range $0{\cdot}15N$ to $0{\cdot}25N$. The wave numbers or frequencies, calculated by equation (12), are in cycle/unit-of-length or cycle/unit-of-time depending on the nature of the spacing δ. The skewness is calculated by equation (9) only for the concentration fields. For velocity fields, the following formula[10] is used instead:

$$\text{Skewness} = \left[(1/N)\sum_{i=1}^{N}(\text{Slope}_i)^3\right] \Big/ \left[(1/N)\sum_{i=1}^{N}(\text{Slope}_i)^2\right]^{3/2}, \tag{15}$$

where

$$\text{Slope}_i = (\alpha_{i+1} - \alpha_{i-1})/2\delta. \tag{16}$$

RESULTS

Optimization of w and p

In order to optimize the values of w and p in equation (3), run number A6 was repeated using a range of values for these parameters. The spatial distribution of the eddy viscosity, K, was calculated at every time step by equation (3). The maximum nodal values were chosen and plotted against time in Figure 3. It is seen that the values $w = 14\delta_x$ and $p = 14\delta_t$ produce the smoothest and best behaved time history of the eddy viscosity K. These values of w and p were used in all the coarse-grid runs.

Mean flow distributions

The results of the runs listed in Table IV are processed as discussed above and plotted in Figures 4–10. Each plot is marked by its run number and compared to the exact averaged data which is marked 'EA'. In Figure 4, the velocity plots marked A1 show clearly that the coarse grid is not suitable for solving the unaveraged equations. Averaging improves the predicted signals by

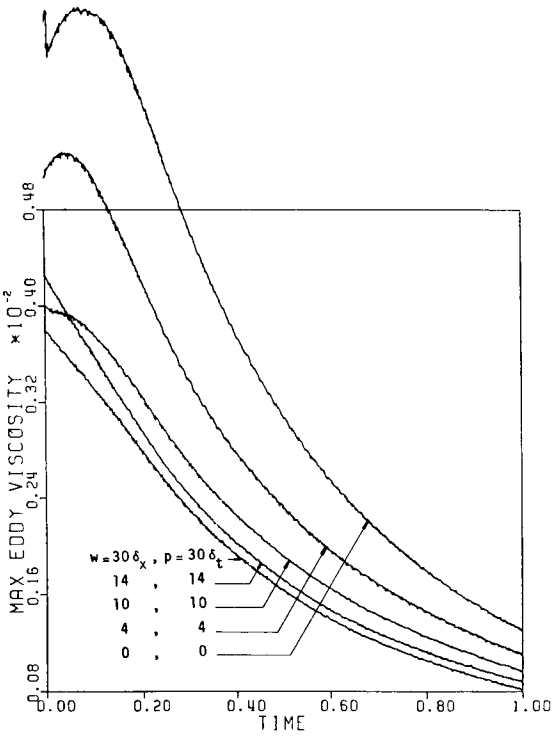

Figure 3. Time behaviour of eddy viscosity as function of w and p

removing the noise from the spatial distributions as well as the time histories of the variables. This smoothing capability clearly increases as the averaging procedure changes from A1 to A6. However inspection of the velocity spatial and temporal distributions in Figure 4 reveal that the new STF filter model results are *smoother* than the A1, A3 results.

Inspection of Figure 5 for the concentration distributions shows the same trend towards increasing agreement with the EA curve with increasing filter complexity. The presence of more 'shock-like' behaviour in the concentration simulation contrasts sharply with the 'wave-like' behaviour in the velocity distributions and represents a serious challenge for the numerical discretizations used in the contaminant equation model. The A6-STF curves do portray the shock behaviour but more high frequency activity is calculated than in the EA curve. Further, the amplitude of the A6 shocks is reduced compared to the EA curves. Of course, some amplitude increase is expected in the EA curve due to the averaging procedure. But the difference noted here cannot be fully explained by the averaging inconsistency.

Spectral behaviour

Figures 6 and 7 show wave number and frequency spectra of the predicted $\bar{u}$ and $\bar{c}$ fields. Observation of the low frequency end of the velocity spectrum reveals that all the model averaging techniques portray the energy peak well both with respect to amplitude and its frequency or wave number of occurrence. For the concentration variance spectra in Figure 7 all the low frequency

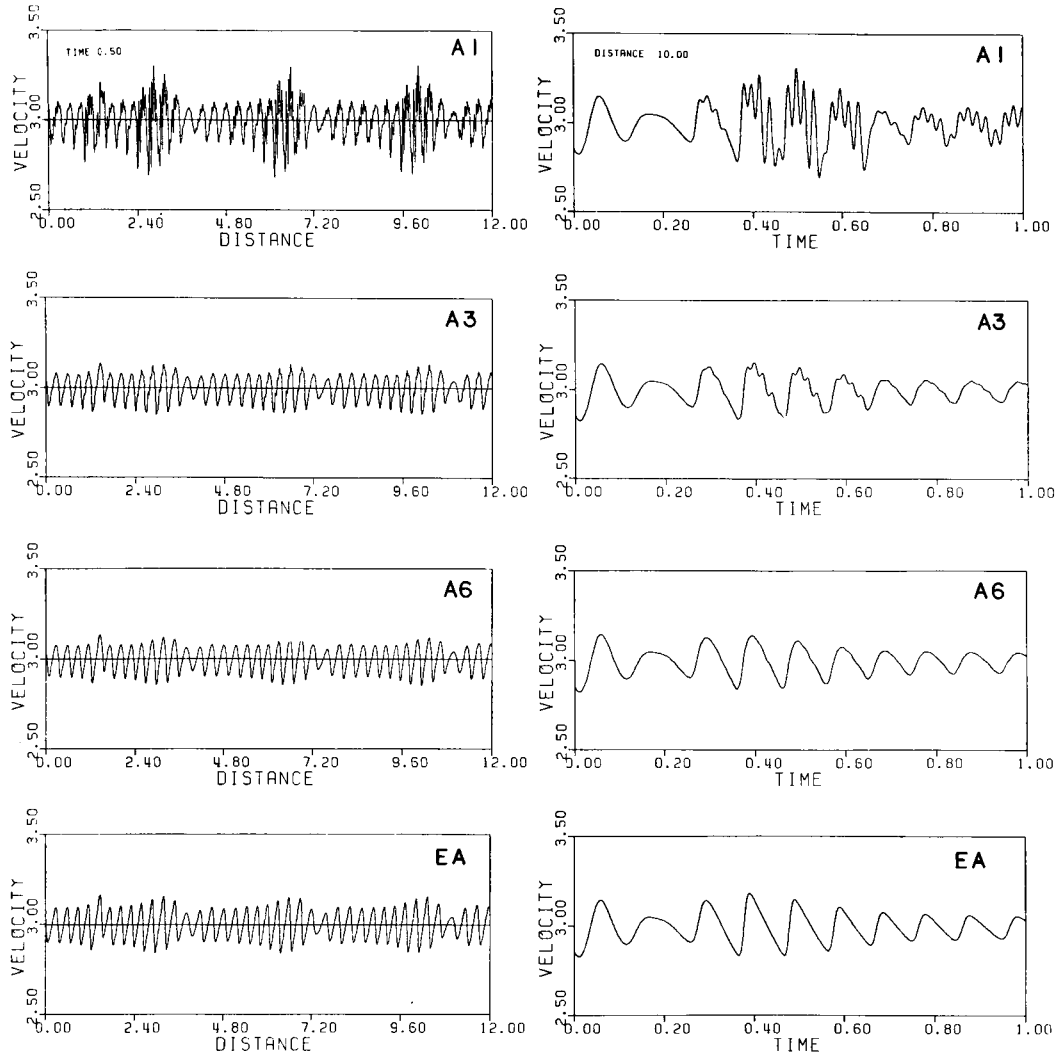

Figure 4. Velocity time and space predictions as functions of averaging method

model spectra have a reduced amplitude compared to the EA, but the occurrence of the maximum variance is as expected. This low frequency amplitude reduction is consistent with the results presented in Figure 5.

The noise in the spatial and temporal distributions in Figures 5 and 6 is depicted in Figures 6 and 7 by the rising tails of the spectral curves. Note that the noise is maximum in run A1 in which the governing equations are not averaged. The Reynolds method of averaging (curves A2) clearly eliminates a large percentage of the noise. With the same grid density, the Leonard's method (curves A3) further improves the results by removing more of the undesirable high frequency and high wave number noise. The best results are obtained by the STF method (curves A4, A5, A6) which introduces the additional temporal filter term. As the filter width Δ_t increases, more noise is eliminated until the 'EA' curves are almost duplicated by A6 in which Δ_t is equal to 10 δ_t. It is

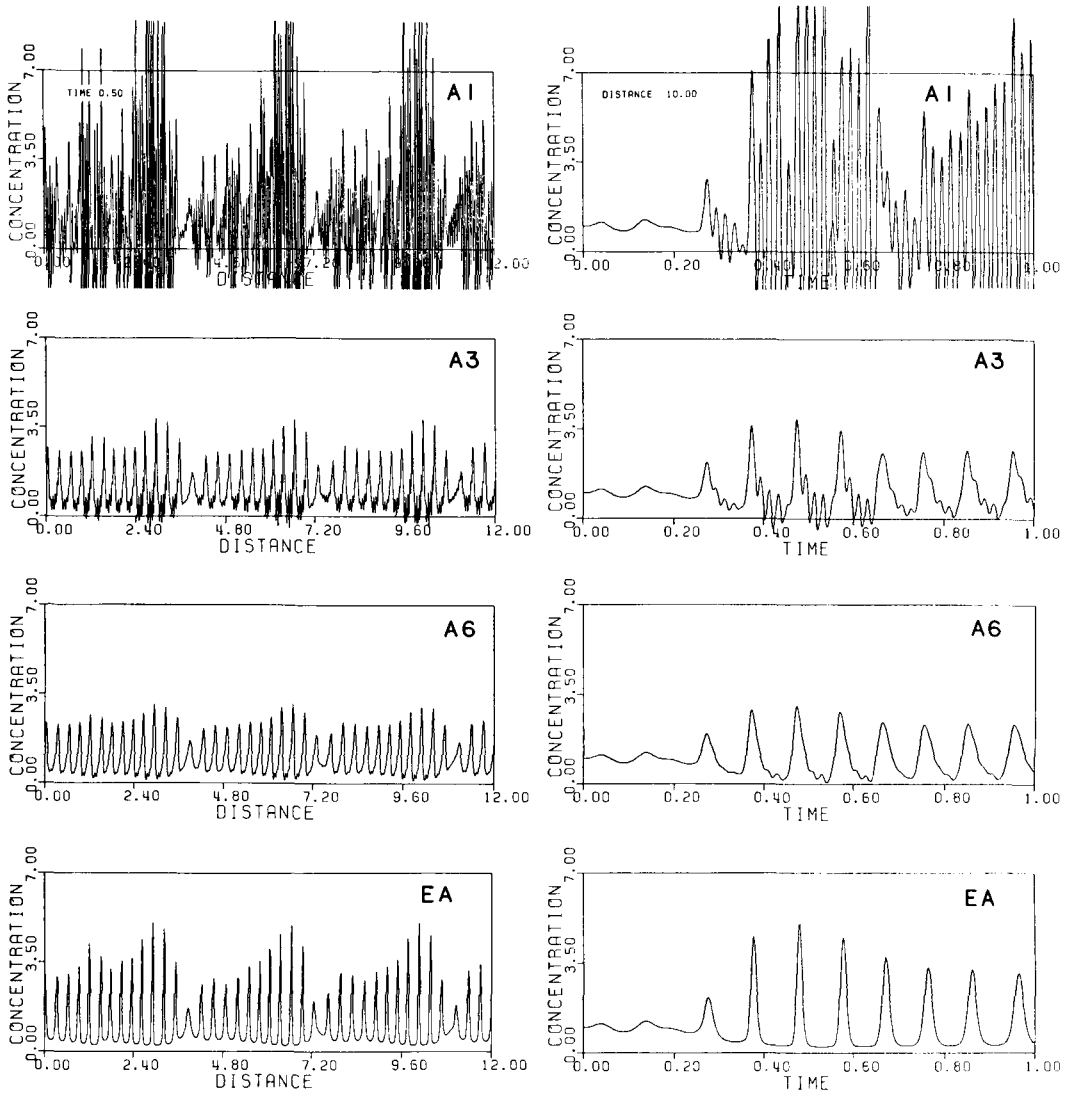

Figure 5. Concentration time and space predictions as functions of averaging method

important to mention that the spectral curves given in Figures 6 and 7 are 'envelopes' to the actual plots which look similar to those given in Part I of this series. The envelopes facilitate drawing and comparing several spectral distributions in one plot.

Another interesting feature in Figures 6 and 7 is the wave number (or frequency) location at which the tails of the spectral envelopes start to rise, indicating a non-plausible calculation. Each averaging method (including no averaging) accurately predicts the portion of $\bar{u}$ and $\bar{c}$ spectra to the left of this location. Since this rising point shifts towards higher wave numbers and higher frequencies as the averaging methods change from A1 to A6, it follows that the new STF method is properly capable of calculating flows with more high frequency or wave number activity than the previous methods are capable of handling with the same grid.

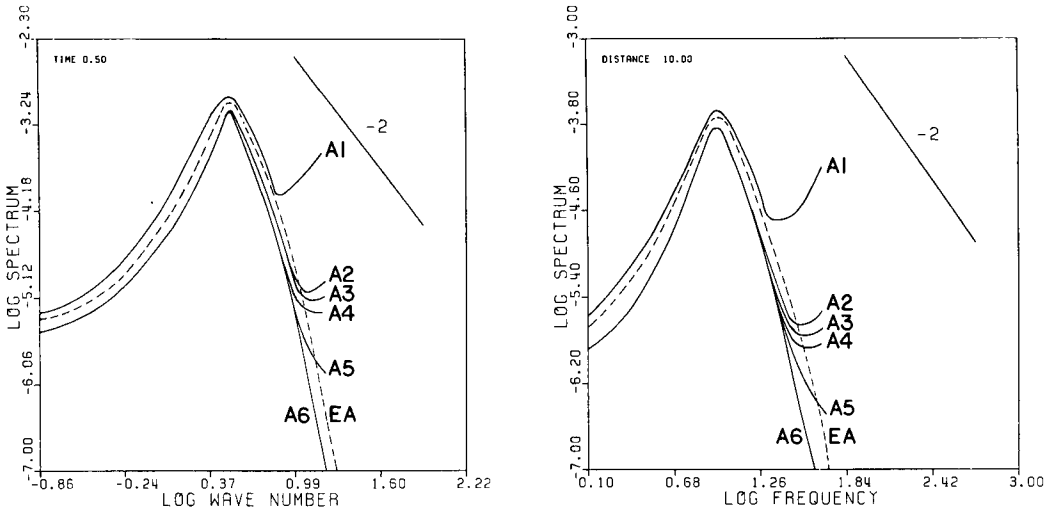

Figure 6. Momentum wave number and frequency spectra as functions of averaging method

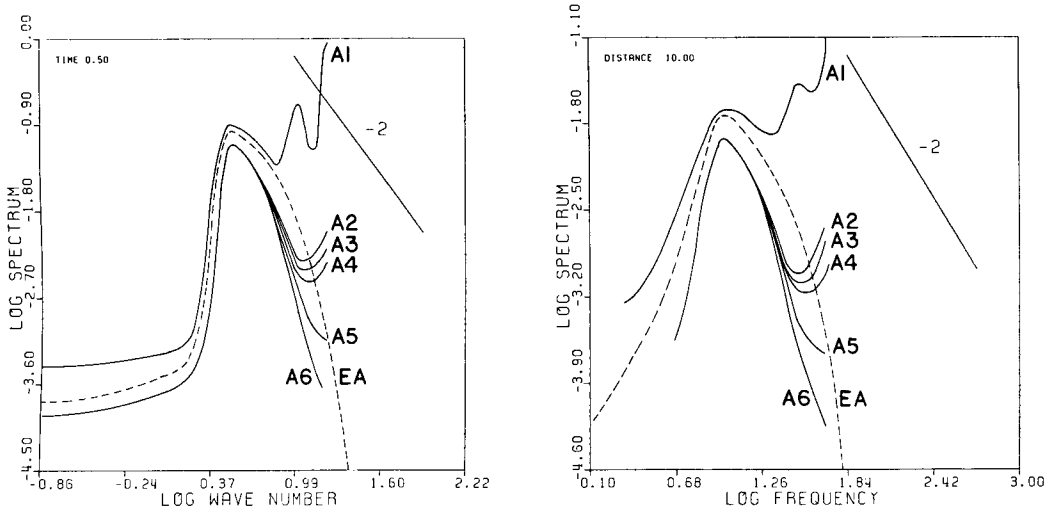

Figure 7. Scalar wave number and frequency spectra as functions of averaging method

Statistical summary

Figure 8 shows time evolution of the $\bar{u}$ statistics as obtained from Table IV runs compared to the exact-averaged data. It is immediately noticed that as expected run A1 (no averaging) results in completely erroneous statistics. Runs A2–A6 give quite similar statistics, which are fairly comparable to their exact-averaged counterparts. In all average forms A2–A6, the skewness is

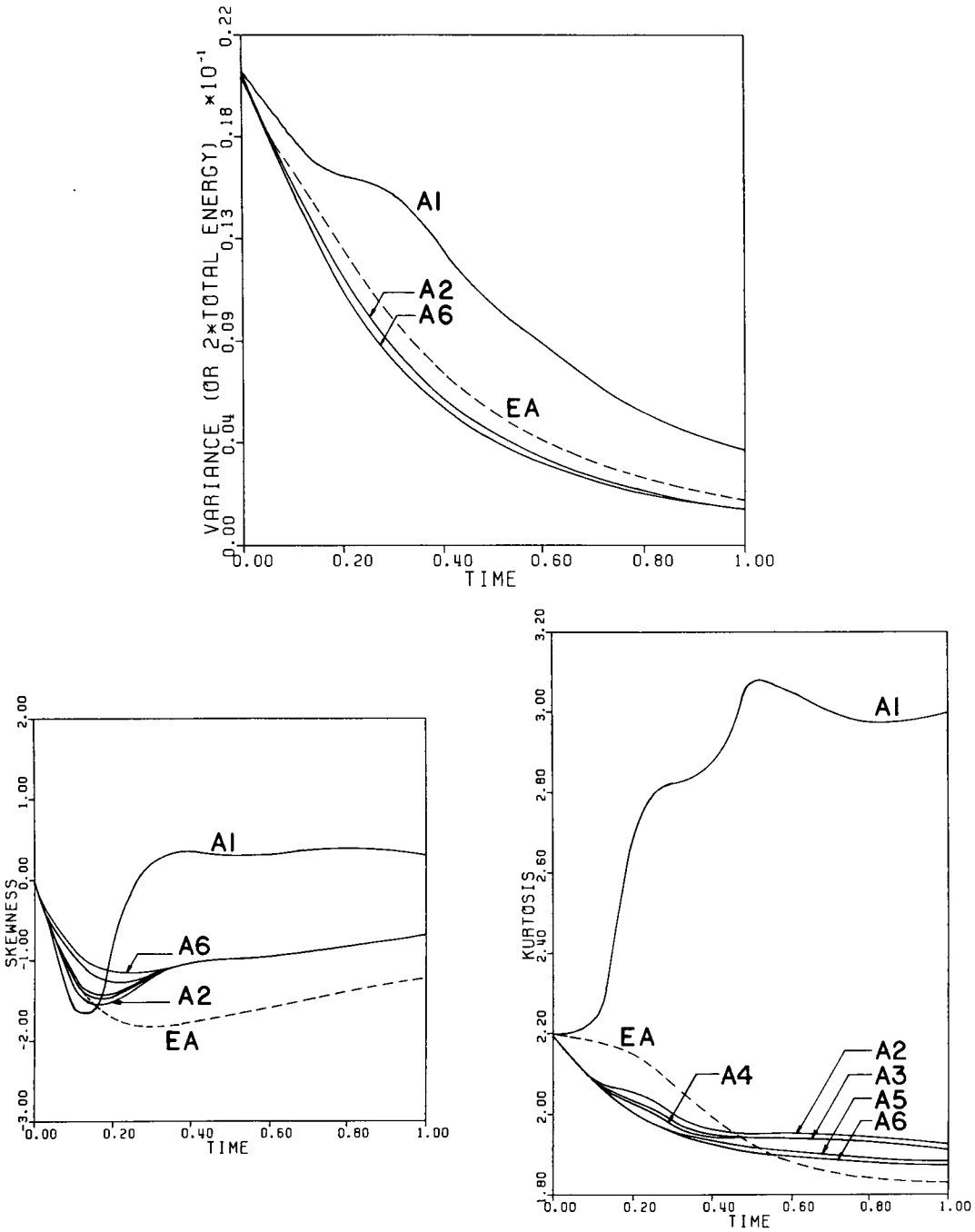

Figure 8. Time behavior of velocity fluctuation statistics as functions of averaging method

overpredicted at longer time and the kurtosis is first underpredicted then overpredicted resulting in a fairly uniform value in time.

The $\bar{c}$ statistics are shown in Figure 9. Again, the A1 curves are in complete disagreement with

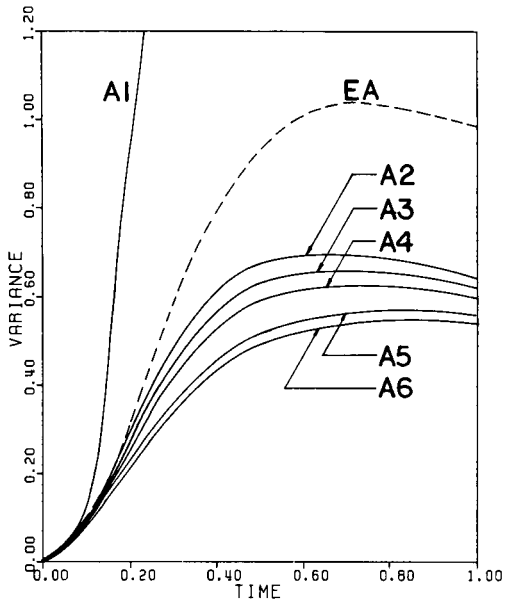

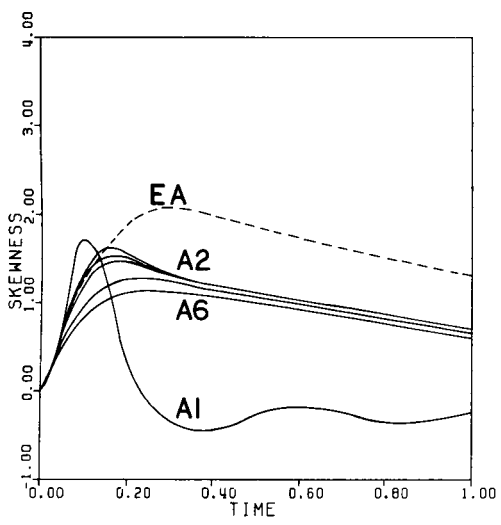

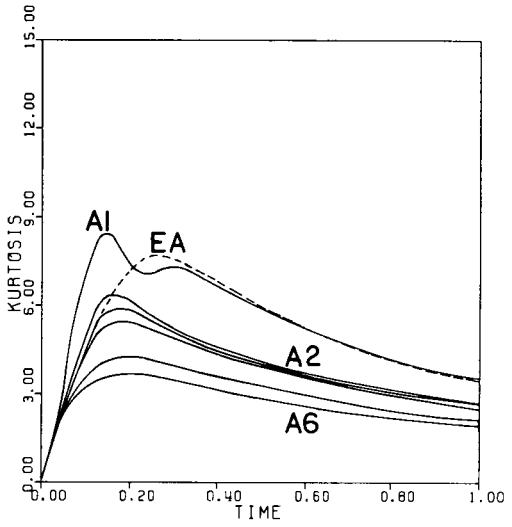

Figure 9. Time behavior of scalar fluctuation statistics as functions of averaging method

the EA curves. Curves A2–A6 are similar and show a behaviour comparable to the EA curves. It is noted that the A2 curves appear to be in a slightly closer quantitative agreement with the exact-averaged data than the A6 curves. This is also true for the $\bar{u}$ statistics shown in Figure 8. The reason is that the EA curves are obtained from the exact u and c signals after averaging them according to the method shown in Figure 2. Had the exact u and c signals been filtered in the same fashion as the equation generating the A3–A6 curves, their deviations from the 'mean' would have been

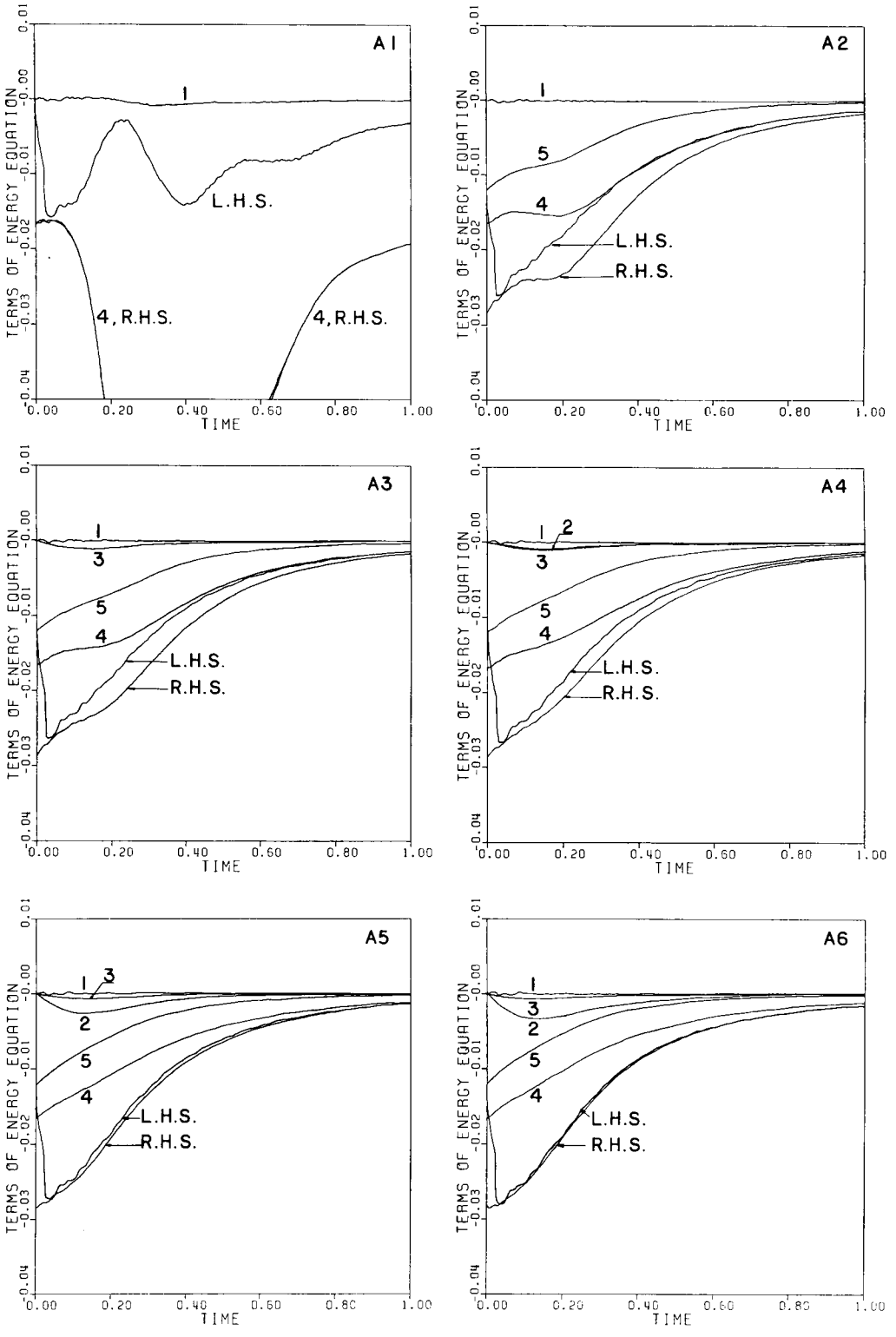

Figure 10. Time behaviour of energy terms (Table III) as functions of averaging method

obviously reduced. This reduction should in turn reduce the magnitudes of the three statistics, which are based on the deviation from the mean, and bring the EA curves closer to the A6 curves. This expected reduction in the magnitudes of the three statistics applies to all the EA curves in Figures 8 and 9 except the velocity skewness in Figure 8. The velocity skewness is calculated by equation (15) rather than the usual skewness formula (9). Since equation (15) does not include the deviations from the mean, the EA skewness may not necessarily be reduced if the exact u and c signals were filtered consistently.

Structure of the energy equation

Figure 10 shows the rewards of improving the averaging method. Time evolutions for each term in the energy equation (Table III) are given for runs A1–A6. The gap between the L.H.S. and the R.H.S. curves in the A1 plot shows the inaccuracy of the calculations. This gap is reduced gradually towards the A6 plot where the L.H.S. and the R.H.S. curves are almost identical. In all plots, the non-linear term (term 1) does not contribute to the energy change at all. The filter terms (terms 2 and 3) are proportional to their respective filter widths. They both start at zero and grow with time to reach a maximum when the shocks are fully developed. Then, the size of the filter terms decreases as the velocity field decays. Note that the temporal filter term is significantly larger than the spatial filter term.

The molecular and turbulent dissipation terms (terms 4 and 5) are governed by R_n and the grid spacings. Since these are constant for all plots in Figure 10, terms 4 and 5 show little change from one plot to another. Note that the major portion of the energy change is caused by the molecular and turbulent viscosity terms, i.e. the SGS motion. The spatial filter terms contribute very little to the dissipation, which implies that they act as a medium for transferring energy from the large-scale to the SGS motion where it is dissipated. However, during the initial and highly transient start-up phase of the calculation the time filter portion is significant in assisting the energy dissipation. It is anticipated therefore that these terms will play such a role in any calculation where the forcing or boundary conditions are dynamic. The excellent agreement between the L.H.S. and R.H.S. total of the energy equation implies excellent conservation of energy capabilities. These authors attribute the very fine agreement to the additional time and space filter. Such energy conservation will allow more accurate long-term calculations.

EVALUATION

The results presented in the preceding section demonstrate that the new space-time filter improves the calculation of transient flows containing variability in the velocity field.

The results demonstrate that, for the range of conditions presented here, the STF prepared models produce greatly improved mean velocity field calculations which include very accurate reproduction of the wave-number spectra. Further, the frequency spectra are also portrayed accurately, indicating that the improvement in the calculation resides in both time and space. The conservation of energy behaviour particularly, with the optimized p and w is exceptional. The structural analyses of the energy equation also reveals that the time filter term plays an important role in the time evolution of the energy distribution and dissipation.

Two features of these results require further elaboration. The first item involves the passive scalar calculation and the necessity of the model to predict 'shock-like' behaviour. Clearly from the EA curves, the expected calculation from the averaged models is the prediction of very high gradient repetitive spikes of concentration. The STF prediction (Figure 5, A6) does reproduce the spikes but with reduced amplitude and increased spread marked by the presence of parasite high

frequency wave activity at the trailing edge of the wave. Two possible sources of these errors exist. The first is that, as noted, a centred approximation for the first order advection term was used. Difficulty in reproducing such high gradient behaviour is often observed[11,12] with centred discretizations containing symmetric coefficients. Therefore for the passive contaminant equation a characteristic-based procedure[13] has been developed and is now being tested for the STF calculations. No such difficulties were noticed in the momentum calculation because the fluctuations were more 'wave-like' and therefore amenable to centred difference discretizations precision in the calculation of high frequency activity.

An additional difficulty in the passive scalar calculation could be the assumption of Clark's reduction. In its original derivation the reduction technique assumed that the fluctuations were wave-like in character. It is apparent that the EA spikes are not wave-like and therefore a possible violation of assumption seems likely. As noted in Table I a form of the STF equations without Clark's reduction was derived and subsequently solved for the conditions described in this paper. The results for the concentration are indistinguishable from those presented here (Figure 5, A6), suggesting that a Clark's reduction is not a problem even for the spike-like behaviour simulated here. The authors conclude that a more effective numerical discretization of the advective term of the scalar transport equation is necessary.

The second item to be discussed is the question of the averaging used to obtain the EA curves. To be completely consistent the averaging method used to prepare each set of model equations should have been used to prepare the exact average data results. To perform space-time or two-dimensional filtering is a convolution problem requiring large computing and financial resources, resources which the authors did not have. Therefore it is possible to ascribe some of the differences between the calculated and EA curves to inconsistent filtering. As per the previous discussion, the authors do attribute the poor statistical results for all model types (except perhaps A1) to the averaging methods. However the averaging problem is confined to those statistical outputs which are quite sensitive to the averaging method. In this case, the spectra calculations are less dependent and the energy structure is independent of the method used to derive the EA, Clearly the improvements in the results are a result of the newer filtering procedure and not a result of an inconsistent averaging preparation of data.

CONCLUSIONS

A new space-time filter has been developed and shows considerable promise in calculating turbulent, fluctuating flow and passive scalar fields. The filter, constructed of Gaussian components in both space and time, results in a sequence of third order terms added to the governing equations which can be reduced in order, without loss of accuracy, by Clark's reduction. Closure by a time and space averaged Smagorinsky model is adequate for the simulations experimented with in this paper.

A filter evaluation procedure based upon a newly derived dynamic 'exact' solution of a Burgers' type equation for momentum and scalar transport proved satisfactory, however the method of reducing the dense 'exact' data to averaged form requires further research. In comparison to calculations made with all other available equation averaging methods the STF permits, for a given coarse grid, improved calculation of (1) the distributions of the time varying dependent variables, (2) the wave number and frequency spectra and (3) the structure the energy equation. The highly improved energy calculation is also marked by a significant contribution from the new terms resulting from the time filter portion of the space-time filter. An improved discretization scheme is required for the first order advection term in the passive scalar equation.

ACKNOWLEDGEMENTS

This work was supported in part by the U.S. National Science Foundation, research grant No. CEE 8410522, and their support is sincerely appreciated. The authors would also like to thank the reviewers for their interesting comments and suggestions.

REFERENCES

1. J. Smagorinsky, 'General circulation experiments with the primitive equations', *Monthly Weather Review*, **93**, (3), 99 (1963).
2. D. K. Lilly, 'On the application of the eddy viscosity concept in the inertial subrange of turbulence' *N.C.A.R. Dept. No. 123*, 1966.
3. D. K. Lilly, 'The representation of small-scale turbulence in numerical simulation experiments', *Proc. IBM Scientific Computing Symposium on Environmental Science*, 1967.
4. D. C. Leslie and G. L. Quarini, 'The application of classical closures to the formulation of subgrid modeling procedures', *J. Fluid Mech.*, **91**, 65 (1979).
5. M. D. Love and D. C. Leslie, 'Studies of subgrid modeling with classical closure and Burgers equation', *Proc. Symp. Turbulent Shear Flows*, University Park, PA, 1977.
6. Y. M. Dakhoul, 'Improved averaging method for turbulent flow simulation', *Ph.D. Thesis*, Ohio State University, 1983.
7. P. J. Roache, *Computational Fluid Dynamics*, Hermosa Publishers, 1972, pp. 222–223.
8. M. D. Love, 'Subgrid modeling studies with Burgers equation', *J. Fluid Mech*, **100**, (1), 87–110 (1980).
9. M. Shinozuka and C. M. Jan, 'Digital simulation of random processes and its application', *J. Sound and Vibration*, **25**, (1), 111–128 (1972).
10. R. A. Clark, J. H. Ferziger, and W. C. Reynolds, 'Evaluation of subgrid-scale turbulence models using a fully simulated turbulent flow', *Rept. TF-9*, Stanford University, Thermosciences Division, 1977.
11. F. M. Holly and Priessmann, 'Accurate calculation of transport in two dimensions', *ASCE J. Hyd. Eng, Div.*, **103**, (HY11), 1259–1277 (1977).
12. A. D. Gosman and K. Lai, 'Finite difference and other approximations for the transport and Navier–Stokes equations', in J. Benque (ed), *Proc. IAHR Symp on Refined Modelling of Flows*, Paris, France, 7–10 September 1982.
13. J. Nocito and K. Bedford, 'Improved solutions for dynamic water quality computations', *Project Completion Rept. NOAA*, (manuscript in preparation), 1985.